

Article

Control Method for Phase-Shift Full-Bridge Center-Tapped Converters Using a Hybrid Fuzzy Sliding Mode Controller

Young Jae Lee , Yeongsu Bak  and Kyo-Beum Lee * 

Department of Electrical and Computer Engineering, Ajou University, 206, World cup-ro, Yeongtong-gu, Suwon 16499, Korea; lzeze93@ajou.ac.kr (Y.J.L.); wov2@ajou.ac.kr (Y.B.)

* Correspondence: kyl@ajou.ac.kr; Tel.: +82-31-219-2487

Received: 15 May 2019; Accepted: 21 June 2019; Published: 22 June 2019



Abstract: This paper presents a control method for phase-shift full-bridge center-tapped (PSFB-CT) converters using hybrid fuzzy sliding mode controllers (SMCs). Conventionally, the output voltage of a PSFB-CT converter is controlled by using a proportional-integral (PI) controller. However, the dynamic characteristic of the converter is undesirable, and the converter is not robust to disturbances. In order to overcome these disadvantages, the SMC based on PI control has been applied for the PSFB-CT converter. However, there is a chattering problem when the SMC gain is increased to improve the dynamic characteristic. In this paper, a control method for the PSFB-CT converter using fuzzy logic control is proposed. By varying the gain of the SMC through the fuzzy logic control, not only can the dynamic characteristic of the PSFB-CT converter be improved, but the chattering problem can also be relieved. The effectiveness of the proposed control method for the PSFB-CT converter was verified by the simulation and experimental results.

Keywords: insulated DC/DC converter; phase-shift full-bridge center-tapped (PSFB-CT) converter; sliding mode controller (SMC); fuzzy logic control

1. Introduction

Recently, the research into electric vehicles (EVs) has gained in popularity and has attracted great attention from research communities [1–3]. Additionally, to cope with a reduction in carbon dioxide and various environmental regulations, the automotive paradigm of the modern society is changing with the development of various EVs. Among the various EVs, pure EVs and plug-in hybrid EVs employ the energy stored in battery packs. Therefore, they require battery packs with much larger sizes and capacities when compared with other EVs. The energy stored in the battery packs is able to supply the power for the electrical equipment of the EVs by using a low DC/DC converter (LDC) [4–6].

The LDC supplies the power from the battery packs with high voltage to the electrical equipment with low voltage. In EVs using the LDC, since the engine power is not consumed in contrast to that of the alternator in a conventional internal combustion generator, the fuel efficiency can be improved. In addition, it has advantages such as miniaturization and weight lightening. Therefore, the research into the topologies and control strategies of the LDC have been actively progressed.

There are many topologies for the LDC that can largely be classified into two types: non-insulated converters and insulated converters. The non-insulated converters for the LDC include the buck and buck-boost converter [7]. The insulated converters for the LDC include flyback, forward, push-pull, half-bridge, and full-bridge converter [8–10]. Among the insulated converters, the flyback, forward, and push-pull converter have disadvantages such as the large size of the transformer and the voltage stress of the switches. In the half-bridge converter, asymmetric control is required to use the zero-voltage

switching (ZVS) method, and causes unbalanced voltage and current stress of the switches. Contrary to other insulated converters, in the full-bridge converter, the ZVS method can be used without asymmetric control thus its control method can be simplified [11]. Therefore, in general, the full-bridge converter is used for the LDC.

Full-bridge converters for the LDC can be classified into resonant full-bridge converters and phase-shift full-bridge (PSFB) converters. The resonant full-bridge converter has a complex system design and it can be difficult to accomplish a wide range of output voltages. In addition, it requires an additional algorithm to control the output voltage at no load system [12,13]. Compared to the resonant full-bridge converter, the system can be designed easily with a PSFB converter and can be achieved with high efficiency because the ZVS method is used by utilizing the resonant inductor and paralleled parasitic capacitor in the PSFB converter. In addition, the PSFB converter has a greater voltage transfer ratio through its transformer galvanic isolation ability [14–18]. In this paper, among the topologies of the various PSFB converters, the PSFB center-tapped (PSFB-CT) converter was used for the LDC.

There are various voltage control methods for the PSFB-CT converter. One of them is a sliding mode controller (SMC) based on PI control. It has a fast-dynamic characteristic and is robust for the disturbance. However, when a gain of the SMC is increased to improve the dynamic characteristic, the output voltage ripple is increased by the chattering problem [19–24]. Therefore, it is important to set an appropriate gain of the SMC, which can reduce the output voltage ripple.

In this paper, the PSFB-CT converter was operated by using the hybrid fuzzy SMC in contrast to other studies that have used the PI controller with implementation convenience to operate the DC-DC converter [15]. Additionally, contrary to other research using the adaptive fuzzy SMC for the general full-bridge converter [25], the hybrid fuzzy SMC proposed in this paper was used for the PSFB-CT converter, and the output voltage of the PSFB-CT converter was controlled by the hybrid fuzzy SMC and the phase-shift between two switch pairs.

This paper presents a control method for a PSFB-CT converter using hybrid fuzzy SMC to improve the dynamic characteristic in comparison to the PI controller in the output voltage control. In the proposed control method, the gain of the SMC is changed by the fuzzy logic control, depending on the magnitude of the output voltage error. Therefore, the LDC using the PSFB-CT converter is able to achieve a fast-dynamic characteristic and decreased output voltage ripple. Additionally, at the same time, the proposed control method based on the SMC has stability and robustness from the disturbance. The effectiveness of the proposed control method for the PSFB-CT converter was verified by the simulation and experimental results.

The rest of this paper is organized as follows: the circuit configuration and operation principle of the PSFB-CT converter are described in Section 2. The control method for the PSFB-CT converter using hybrid fuzzy SMC is proposed and analyzed in Section 3. In Sections 4 and 5, the simulation and experimental results are implemented and provided to verify the effectiveness of the proposed control method, respectively. Finally, the conclusion of this research is given in Section 6.

2. Circuit Configuration and Operation Principle of PSFB-CT Converter

2.1. Circuit Configuration

Figure 1 shows the circuit configuration of the PSFB-CT converter, which is composed of a full-bridge converter, transformer, and center-tapped rectifier. The full-bridge converter consists of four switching devices and converts the input DC voltage into AC voltage as the square waveform, and the power of the input stage is transferred to the transformer. In addition, the center-tapped rectifier consists of two diodes and converts the AC voltage that is delivered through the transformer to the output DC voltage.

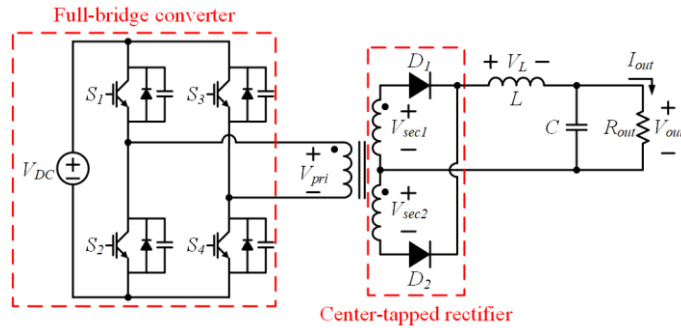


Figure 1. Circuit configuration of the PSFB-CT.

2.2. Operation Principle

In the PSFB-CT converter, a duty ratio of the full-bridge converter is fixed as 0.5 and the output voltage is determined by the phase-shift between a switch pair of S_1 and S_4 and the other switch pair of S_2 and S_3 . The duty section of the switch pair, which is overlapped by the phase-shift, produces the AC voltage [26,27]. The AC voltage is applied to the primary side of the transformer. As a result, the full-bridge converter can perform a soft switching of the switching devices without an additional circuit, simply by placing the phase-shift on the gate signal of the switching devices.

The transformer located between the full-bridge converter and center-tapped rectifier transfers the electrical energy. In other words, the primary voltage of the transformer obtained by the operation of the full-bridge converter is transferred to the secondary side, which is connected to the center-tapped rectifier. Finally, the secondary voltage of the transformer becomes the output DC voltage of the PSFB-CT converter.

Figure 2 shows the equivalent circuits of the PSFB-CT converter depending on the operation of the switches. There are four different operation modes and the primary voltage (V_{pri}) of the transformer has three different levels depending on the modes. In Mode 1, the S_1 and S_4 are in the ON state. Therefore, the V_{pri} of the transformer has a positive value and the upper diode (D_1) is ON state. In the Mode 2 and Mode 4, the S_1-S_3 and S_2-S_4 are ON state, respectively and the V_{pri} and the secondary voltage (V_{sec1} and V_{sec2}) of the transformer is 0 V. In addition, in contrast to Mode 1, the S_2 and S_3 are in an ON state in Mode 3. The V_{pri} of the transformer has a negative value and the lower diode (D_2) is ON state. Finally, in both Modes 1 and 3, the secondary voltage (V_{sec1} and V_{sec2}) of the transformer is decreased by the turn ratio of the transformer.

In Figure 2, the voltage applied to the inductor (L) is expressed as Equation (1).

$$V_L = nV_{DC} - V_{out}, \quad (1)$$

where n is the turn ratio of the transformer; V_{DC} is input DC voltage; and V_{out} is output DC voltage.

Depending on the voltage-second balance method regarding the V_L as the inductor voltage, a voltage transfer ratio of the PSFB-CT converter is expressed as Equation (2) [28].

$$\begin{aligned} V_L \cdot DT &= (nV_{DC} - V_{out}) \cdot DT = V_{out} \cdot \left(\frac{T}{2} - DT \right), \\ \frac{V_{out}}{V_{DC}} &= 2nD, \end{aligned} \quad (2)$$

where D is the duty ratio of the full-bridge converter and T is the sampling period.

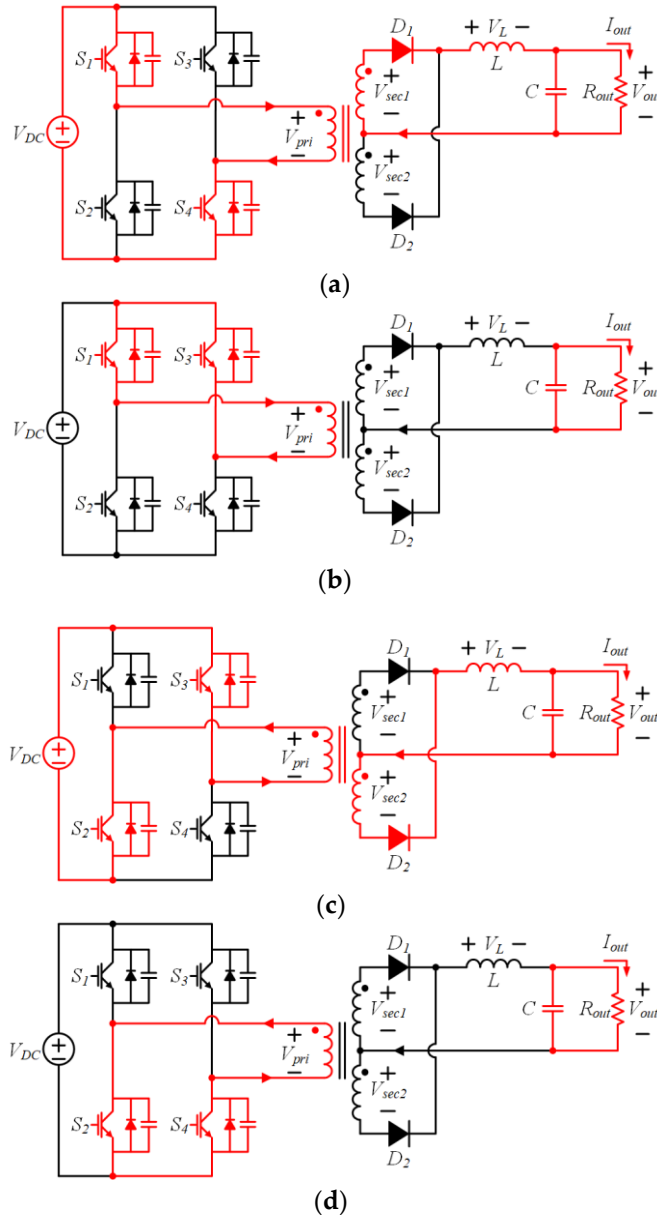


Figure 2. Equivalent circuits of the PSFB-CT converter depending on the operation of switches. (a) Mode 1; (b) Mode 2; (c) Mode 3; (d) Mode 4.

3. Proposed Control Method for PSFB-CT Converter Using Hybrid Fuzzy SMC

3.1. Output Voltage Control Using the SMC

The SMC is a type of various variable structure controller (VSC) and is a non-linear control method. The SMC for the PSFB-CT converter has an error trajectory of the variables such as output voltage and current, which need to be controlled. The error trajectory reaches the sliding plane by a proper control input of the SMC. Once the error trajectory of the PSFB-CT converter is applied to the input of the sliding plane, the SMC for the PSFB-CT converter is robust to internal parameter variation and external disturbance. In the SMC represented by either a linear or nonlinear high-order differential equation, the differential equation of the sliding mode can be entirely independent of effects due to internal parameter variation and external disturbance [29,30]. Therefore, the sliding mode is said to be robust to internal parameter variation and disturbance [29,30]. Therefore, it is possible to effectively control

the variables of the PSFB-CT converter and achieve robust control performance without accurate mathematical modeling of the converter.

Figure 3 shows the proposed control block diagram of the PSFB-CT converter using hybrid fuzzy SMC. First, in the SMC, an output voltage error (e_V) is calculated by the difference between the reference output voltage (V_{out}^*) and the real output voltage (V_{out}) of the PSFB-CT converter. This is applied to the input of the SMC and a sliding plane of the SMC is obtained by the e_V . Since the sliding plane is an important variable that determines the control performance of the SMC, it is designed by various forms suitable for each system [19,22–24]. In this paper, it was designated as *Surface*, which is designed with the e_V and its integral term as Equation (3).

$$Surface = e_V + k \int e_V dt, \quad (3)$$

where k is a sliding coefficient, which is set to 1 in this paper.

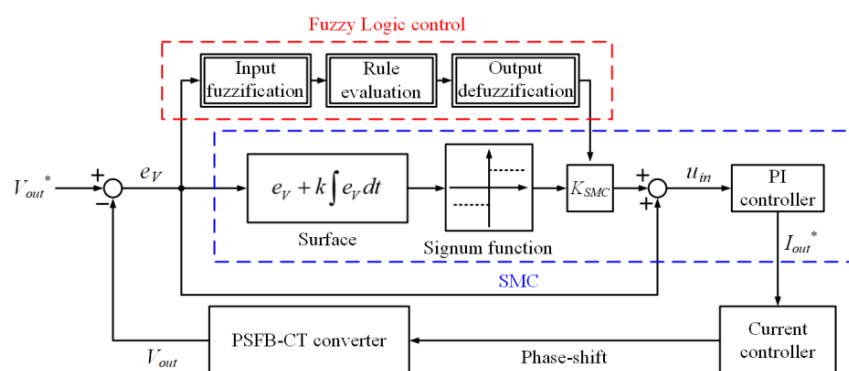


Figure 3. Proposed control block diagram of the PSFB-CT converter using hybrid fuzzy SMC.

The *Surface* passes the signum function to relieve the chattering phenomenon, which is expressed as Equation (4).

$$\text{sgn}(Surface) = \begin{cases} 1, & Surface > 0 \\ 0, & Surface = 0 \\ -1, & Surface < 0 \end{cases}. \quad (4)$$

Additionally, the error (e_{VSC}) of the VSC using the SMC is obtained through the $\text{sgn}(Surface)$ multiplies by the gain (K_{SMC}) of the SMC. Finally, the input of the PI controller in the SMC is formed in parallel with the e_V and e_{VSC} as in Equation (5).

$$u_{in} = e_V + e_{VSC} = e_V + K_{SMC} \text{sgn}(Surface). \quad (5)$$

The u_{in} is controlled to zero by the PI controller and the reference output current (I_{out}^*) is obtained as a result of the SMC.

The output current (I_{out}) of the PSFB-CT converter is controlled to the I_{out}^* by the current controller based on the PI control, which is modeled as an inner loop of the proposed hybrid fuzzy SMC for the output voltage control. In order to design the current controller based on the PI control, in general, the linearized model of the PSFB-CT converter should be determined by using a small signal analysis in general. In addition, since the PSFB-CT converter contains a center-tapped rectifier, the small signal analysis of the PSFB-CT converter is modeled with the synchronous buck converter as a form of two phase interleaved. By using the small signal analysis, the output voltage and current of the PSFB-CT converter are modeled linearly. As a result, the transfer function of the current controller, which controls the output current, is represented by the linearized model of the output voltage and current [31]. Finally, a phase-shift is obtained as a result of the current controller and the PSFB-CT converter drives using the phase-shift.

In the SMC, as shown in Figure 3, the u_{in} is composed of the e_V and e_{VSC} that lead to the formation of a linear structure and the VSC, respectively. Therefore, the SMC for the PSFB-CT converter has a fast dynamic characteristic and is robust to internal parameter variation and external disturbance [29]. However, in the case where the K_{SMC} is increased to achieve the fast dynamic characteristic of the SMC for the PSFB-CT converter, the ripple of the V_{out} is also increased due to the chattering phenomenon, which causes an unstable system. Therefore, in order to supplement this disadvantage of the SMC, the K_{SMC} was properly changed by the fuzzy logic control with the e_V in the proposed control method as shown in Figure 3.

3.2. Stability Analysis of the Hybrid Fuzzy SMC

The transfer function of the PSFB-CT converter is necessary to analyze the stability of the hybrid fuzzy SMC for the PSFB-CT converter. However, it is difficult to obtain the accurate transfer function of that considering the operating modes. Therefore, in this paper, the hybrid fuzzy SMC for the PSFB-CT converter is treated as a black-box model, which is able to analyze with only input and output discrete data. In order to analyze the discrete data, in this paper, the least square parameter estimation algorithm is used [32,33]. As a result, the discrete transfer function of the hybrid fuzzy SMC can be built based on the results of the parameter estimation. It is converted to a continuous transfer function, which is expressed as in (6), using the zero-order-hold method [33].

$$\begin{aligned} H(s) &= \frac{b_1 s^3 + b_2 s^2 + b_3 s^1 + b_4}{s^4 + a_1 s^3 + a_2 s^2 + a_3 s^1 + a_4} \cdot \left(k_{vps} + \frac{k_{vis}}{s} \right) \cdot \left(k_{cps} + \frac{k_{cis}}{s} \right) \\ &= \frac{5.508e5s^3 + 6.664e10s^2 + 2.175e17s^1 + 4.777e21}{s^4 + 4.846e5s^3 + 1.64e11s^2 + 4.666e15s^1 + 1.07e19} \cdot \left(k_{vps} + \frac{k_{vis}}{s} \right) \cdot \left(k_{cps} + \frac{k_{cis}}{s} \right), \end{aligned} \quad (6)$$

where k_{vps} and k_{vis} are proportional and integral gain of the voltage controller based on the hybrid fuzzy SMC, respectively. In addition, k_{cps} and k_{cis} are proportional and integral gain of the current controller based on the PI control, respectively. By using the $H(s)$ as in (6), the stability of the hybrid fuzzy SMC can be analyzed with the bode diagram and the poles and zeros on complex plane as follows.

Figure 4 shows the bode diagram of the transfer function $H(s)$. In the $H(s)$, the k_{vps} , k_{vis} , k_{cps} , and k_{cis} are set to 0.995456, 2816, 0.00658924, and 2.33, respectively. In Figure 4, the crossing frequency is about 10,000 rad/s, the gain margin (GM) is 41 dB, and the phase margin (PM) is 108°. Therefore, through the stability analysis using the bode diagram, it is proved that the hybrid fuzzy SMC for the PSFB-CT converter is stable.

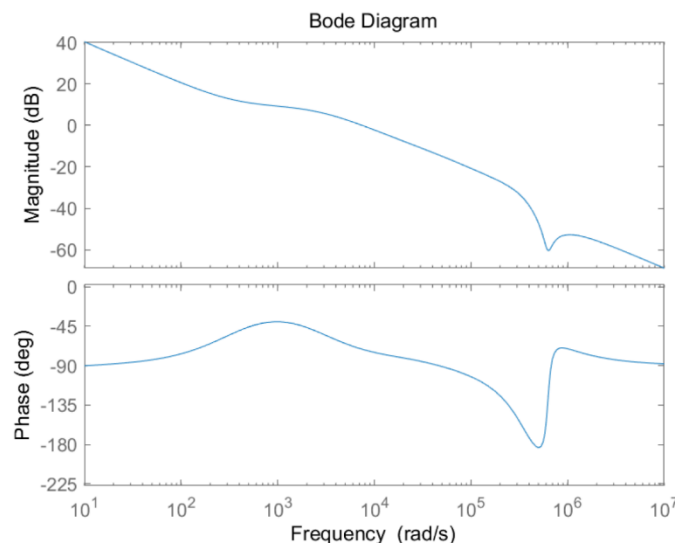


Figure 4. Bode diagram of the transfer function $H(s)$.

In addition, Figure 5 shows the poles and zeros of the transfer function $H(s)$ on complex plane. In Figure 5, all of the poles are positioning in the left half plane (LHP). Therefore, through the stability analysis using the poles and zeros on complex plane, it is also proved that the hybrid fuzzy SMC for the PSFB-CT converter is stable.

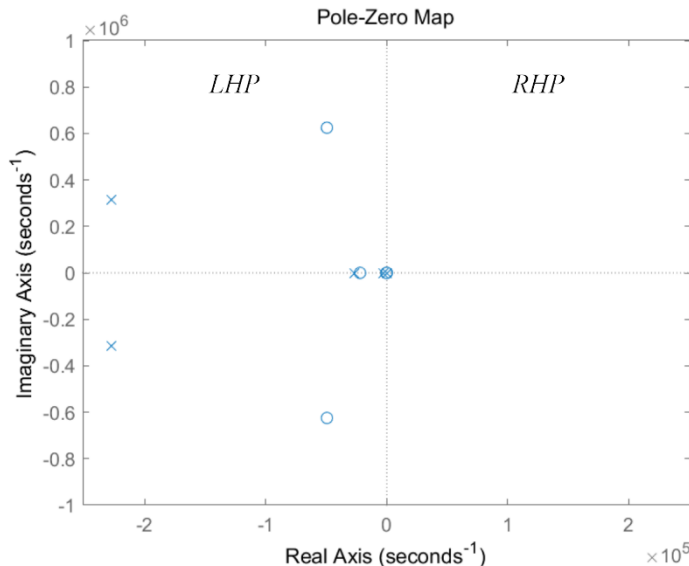


Figure 5. Poles and zeros of the transfer function $H(s)$ on complex plane.

3.3. Design of Fuzzy Logic Control

The fuzzy logic control is one of the control methods based on a mathematical system analyzing analog values. Figure 6 shows the data flow of the fuzzy logic control. It is mainly classified into three major transformations: an input fuzzification, a rule evaluation, and an output defuzzification. By using the three major transformations in the data flow of the fuzzy logic control, the system output of the fuzzy logic control can be obtained from the system input [34–38]. In other words, in this paper, the system input and output were the e_V and the K_{SMC} , respectively. As a result, the appropriate K_{SMC} for reducing the ripple of the V_{out} depending on the e_V can be obtained by using the fuzzy logic control.

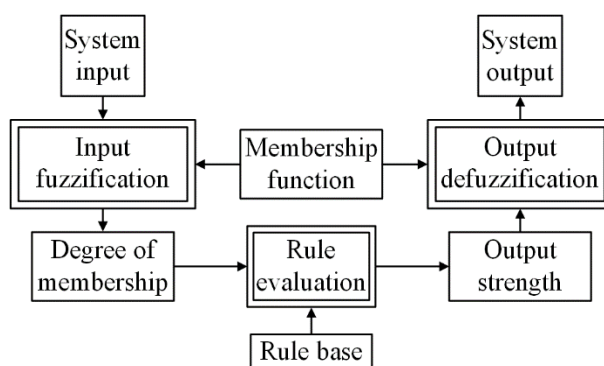


Figure 6. Data flow of the fuzzy logic control.

The input fuzzification is the process that the system input assigns to one or several membership functions, which are pre-defined depending on the value of the system input. The number and shape of the membership function determine the dynamic characteristic and stability of the fuzzy logic control. Through input fuzzification using the membership function, a degree of membership (DOM) is obtained, which indicates the degree of belonging for each system input to the membership function. The rule evaluation is the process that an output strength based on the DOM is decided

by using the if-then grammar. The output strength indicates an influence of the system input that affects the system output. Finally, the output defuzzification is the process that produces a quantifiable result in the fuzzy logic control and calculates the system output of the fuzzy logic control by using the pre-defined membership function, corresponding DOM, and output strength. In this paper, the center of gravity (COG) defuzzification method is used for the fuzzy logic control because it is the most popular defuzzification method [39]. In the COG defuzzification method, the system output is calculated as a sum of multiplication between the DOM and the corresponding output strength.

3.4. Variation of the K_{SMC} Using Fuzzy Logic Control

In fuzzy logic control, recently, research regarding the shape of the membership function has actively progressed [40]. Figure 7 shows the various shapes of the membership function such as triangular, trapezoidal, polygonal, and Gaussian. However, except for the triangular membership function, the others are complicated in terms of implementation.

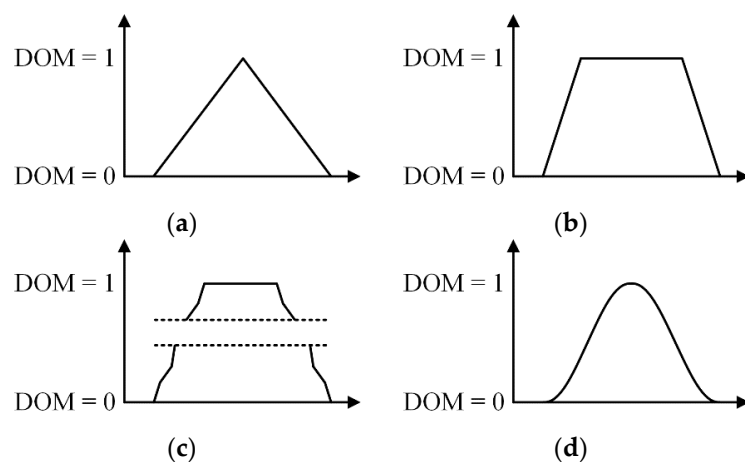


Figure 7. Various shapes of membership function. (a) Triangular; (b) Trapezoidal; (c) Polygonal; (d) Gaussian.

The performance of the fuzzy logic control using the trapezoidal membership function is almost the same as that using the triangular membership function. However, the trapezoidal membership function is hard to implement when compared with the triangular membership function. In addition, the fuzzy logic control using the triangular membership function has no overshoot and fast dynamic characteristic when compared with that obtained when using the others [41]. Therefore, in this paper, the triangular membership function with an advantage of convenience of implementation was adopted among various shapes of the membership function [34,36].

The number and values of the triangular membership function should be set properly in order to achieve outstanding performance of the fuzzy logic control. The performance of the fuzzy logic control with a number of the membership functions can be improved, however, it has a computation burden. Therefore, in this paper, the number of the membership function was set to five. Additionally, the values of the membership function are determined by experiences and intuitions because the fuzzy logic control is readily customized in human language terms. The output voltage error of 6 V is considered as a large error. Therefore, in this paper, 6 V and -6 V were the values of the triangular membership function allocated as the big positive and negative values, respectively. In addition, the output voltage error of 1 V is considered as a small error, therefore, 1 V and -1 V were the values allocated as the small positive and negative values, respectively.

Figure 8 shows the membership functions with the DOM. In this paper, the number of membership functions was set to five and their shape was constructed as a triangle. The five membership functions were composed of NN, N, Z, P, and PP and the DOM was set as zero to 1. The definition of the

membership functions is listed in Table 1. NN and N represent the big and small negative values, which were set to -6 and -1 , respectively. Z is the nearly zero and was set as zero. In addition, PP and P were the big and small positive values, which were set as 6 and 1 , respectively. In this paper, the values of the membership functions indicate the e_V as the output voltage error.

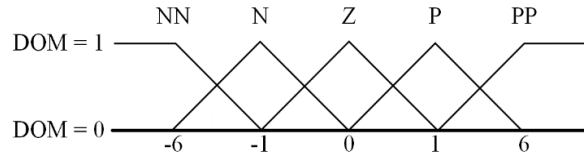


Figure 8. Membership functions with the DOM.

Table 1. Definition of membership functions.

Membership Function	Meaning	Value
NN	Big negative value	-6
N	Small negative value	-1
Z	Nearly zero	0
P	Small positive value	1
PP	Big positive value	6

Figure 9 shows the output strength based on the DOM depending on the membership function. The output strength was set to 40 , 5 , and 1 using the rule evaluation as If-Then grammar:

- If the e_V is very large as positive, Then the K_{SMC} is very large.
- If the e_V is slightly large as positive, Then the K_{SMC} is slightly small.
- If the e_V is nearly zero, Then the K_{SMC} is nearly zero.
- If the e_V is slightly large as negative, Then the K_{SMC} is slightly small.
- If the e_V is very large as negative, Then the K_{SMC} is very large.

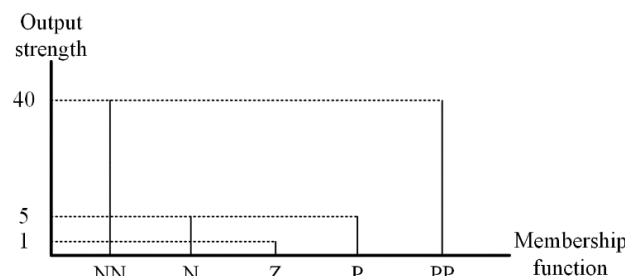


Figure 9. Output strength based on the DOM depending on the membership function.

As a result, with the above rule evaluation, the K_{SMC} can be properly changed smoothly depending on the e_V .

In this paper, through the proposed control method for the PSFB-CT converter using the hybrid fuzzy SMC, the ripple of the V_{out} could be reduced and the dynamic characteristic improved.

The proposed hybrid fuzzy SMC is different from a look-up table, which is just an array that replaces runtime computation with a simple array. Contrary to the K_{SMC} , which is discontinuously changed depending on the look-up table, the K_{SMC} in the proposed hybrid fuzzy SMC is continuously changed by its feedback. Therefore, the K_{SMC} in the proposed hybrid fuzzy SMC is adequate compared with that in the look-up table.

4. Simulation Results

In order to verify the effectiveness of the proposed hybrid fuzzy SMC, a simulation was performed using PSIM software. The simulation circuit diagram was designed as the configuration of the PSFB-CT converter, as shown in Figure 1. The input DC voltage (V_{DC}) was set to 300 V and the additional simulation parameters are given in Table 2. In the voltage controller based on the hybrid fuzzy SMC, the proportional and integral gain are set to 0.995456 and 2816, respectively. Additionally, in the current controller based on the PI control, the proportional and integral gain were set to 0.00658924 and 2.33, respectively.

Table 2. Simulation parameters.

Parameters	Value
Input DC voltage (V_{DC})	300 V
Transformer turn ratio (n)	87:12
Output capacitor (C)	176 μ F
Output inductor (L)	9.32 μ H
Output resistor (R_{out})	1 Ω
Control period (T)	12.5 μ s

Figure 10 shows the simulation results about operation principle of the PSFB-CT converter. It indicates (a) the operation status of S_1 and (b) S_3 , (c) primary (V_{pri}), and (d) secondary voltage (V_{sec1}) of the transformer, and (e) output DC voltage (V_{out}) and reference output voltage (V_{out}^*). The phase-shift between S_1 and S_3 makes the V_{pri} . Since the V_{DC} was set to 300 V, the V_{pri} was 300 V peak and was reduced to V_{sec1} , which was 41 V_{peak} by the transformer turn ratio of 87:12. Additionally, the V_{sec1} as the pulse waveform became V_{out} through the center-tapped rectifier. The V_{out} was controlled to the V_{out}^* , which was set to 15 V.

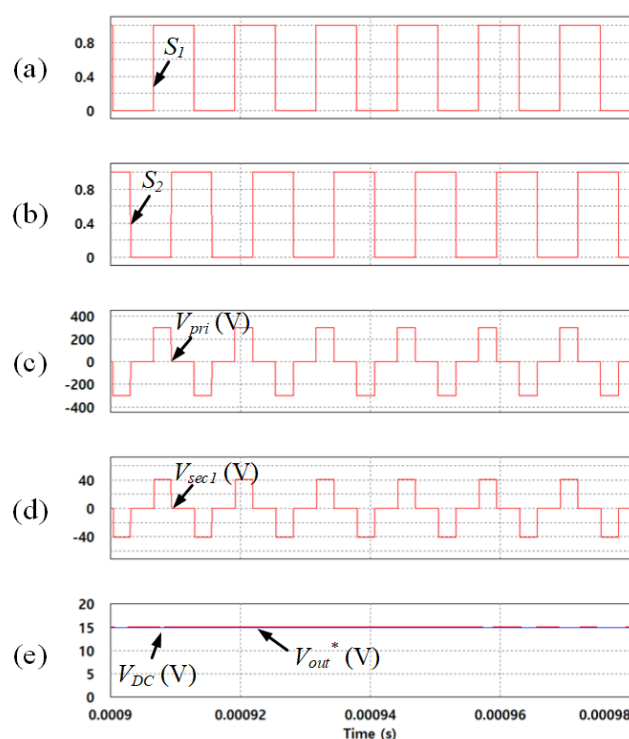


Figure 10. Simulation results about operation principle of the PSFB-CT converter. (a) Operation status of S_1 ; (b) Operation status of S_3 ; (c) Primary voltage of the transformer; (d) Secondary voltage of the transformer; (e) Output DC voltage and reference output voltage.

Figure 11 shows the simulation results of the PSFB-CT converter using the SMC depending on K_{SMC} , which was set to (a) 0, (b) 1, and (c) 3, respectively. The V_{out}^* was changed to 15 V from 10 V at 0.01 s and the V_{out} was controlled to V_{out}^* . In Figure 11a, the evsc in u_{in} as in (5) became a zero because the K_{SMC} is 0. Therefore, the SMC was performed the same as the PI controller. In contrast to Figure 11a, in Figure 11b,c, the dynamic characteristic of the PSFB-CT converter was improved because the K_{SMC} increased to 1 and 3, respectively. However, in these results, the output voltage and current ripple increased at the same time.

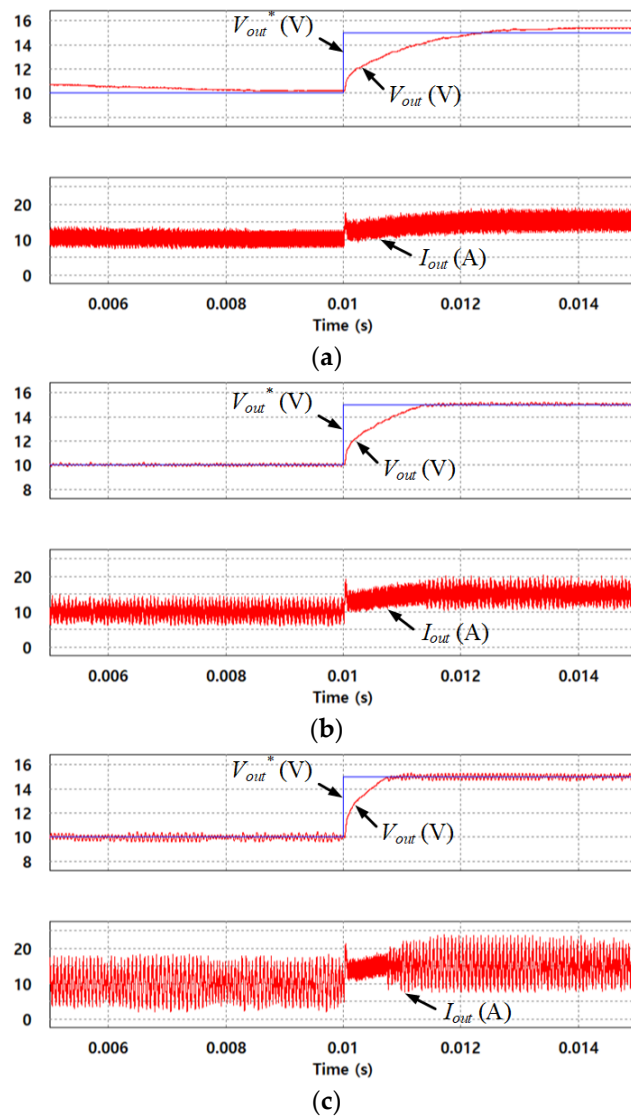


Figure 11. Simulation results of the PSFB-CT converter using the SMC depending on K_{SMC} . (a) $K_{SMC} = 0$; (b) $K_{SMC} = 1$; (c) $K_{SMC} = 3$.

Using the same scenario as that in Figure 11, Figure 12 shows the simulation results of the PSFB-CT converter using three different controllers: (a) the PI controller, (b) SMC, and (c) proposed hybrid fuzzy SMC. In Figure 12a with the PI controller, the dynamic characteristic of the PSFB-CT converter was undesirable, where the settling time was about 2 ms. In the steady state, the output voltage ripple was nearly zero and the output current ripple was relatively small. In Figure 12b with the SMC, the dynamic characteristic of the PSFB-CT converter was improved, where the settling time was about 0.8 ms when compared to that of the PI controller as shown in Figure 12a. However, in the steady state, the output voltage and current ripple were increased by the chattering phenomenon. Finally, in

Figure 12c with the proposed hybrid fuzzy SMC, the dynamic characteristic of the PSFB-CT converter was also improved, where the settling time was about 0.9 ms when compared with the PI controller. It was desirable compared to the SMC. In the proposed hybrid fuzzy SMC, the K_{SMC} is properly varied depending on the output voltage error. As a result, the dynamic characteristic of the PSFB-CT converter is improved and the output voltage and current ripple are decreased by varying the K_{SMC} .

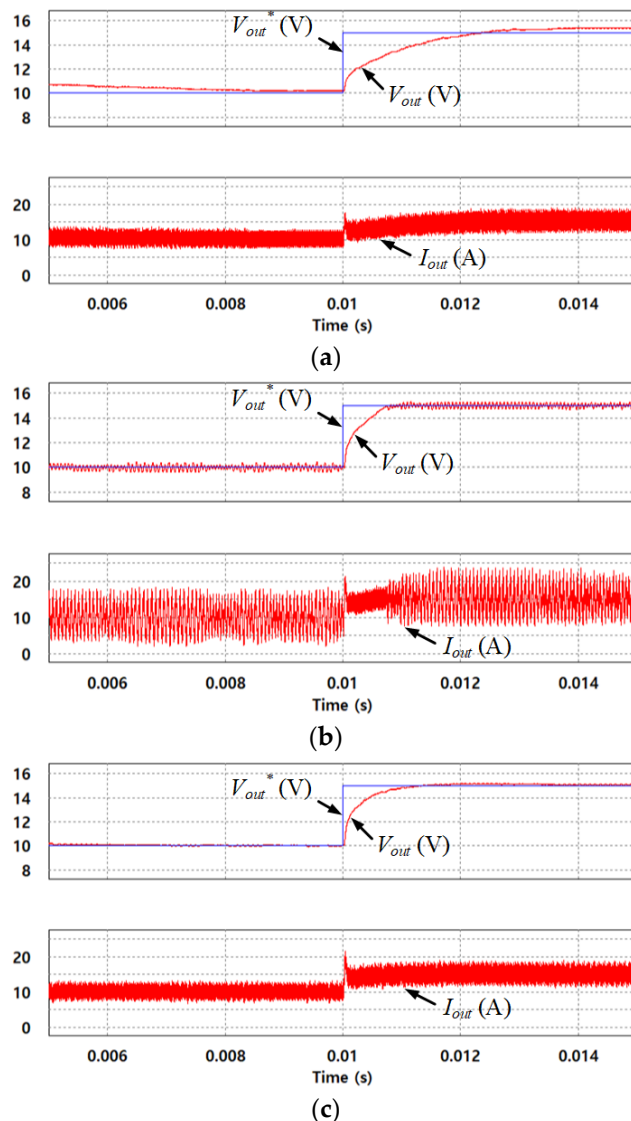


Figure 12. Simulation results of the PSFB-CT converter using three different controllers. (a) PI controller; (b) SMC; (c) proposed hybrid fuzzy SMC.

5. Experimental Results

In order to demonstrate the performance of the proposed control method for the PSFB-CT converter using the hybrid fuzzy SMC, experiments were conducted. Figure 13 shows the experimental setup, which was composed of a control board, a power board, transformer, and center-tapped rectifier. The power for the experimental setup was generated by the switching mode power supply (SMPS) of Power Plaza, Seoul, Korea. The control board consisted of a micro controller unit (MCU) using the SPC570S50E1 of ST microelectronics, Geneva, Switzerland. The control method for the PSFB-CT converter using the proposed hybrid fuzzy SMC was programmed on the MCU. The control board obtained the signals from the input–output voltage and current sensors to control the PSFB-CT converter and transferred the PWM signals obtained from the proposed hybrid fuzzy SMC to the power board.

Additionally, the V_{pri} was generated by the operation of the PSFB-CT converter in the power board, which was composed of four MOSFETs using a SCT3030KL of a ROHM semiconductor, Kyoto, Japan. Finally, through the transformer of Chang Sung electronics, Gunpo, Korea, and the center-tapped rectifier composed of two diode-modules using STPS200170TV1Y of ST microelectronics, Geneva, Switzerland, the V_{out} came out, which connected to the resistance load. The experimental parameters were the same as the simulation parameters given in Table 2.

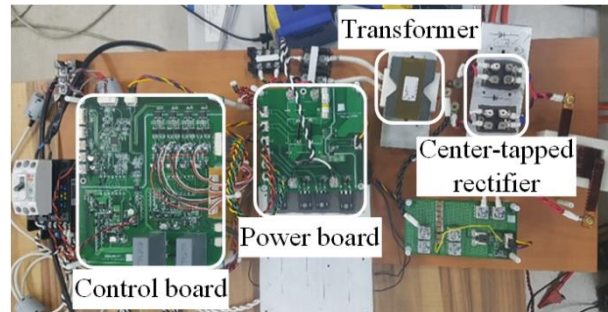


Figure 13. Experimental setup.

Figure 14 shows the experimental results on the operation principle of the PSFB-CT converter when the V_{out}^* was 15 V and indicates the gate signals (S_1_signal and S_3_signal) of S_1 and S_3 , the primary voltage (V_{pri}), and secondary voltage (V_{sec1}). The phase-shift between S_1 and S_3 makes the V_{pri} , which is transferred to the secondary side of the transformer as the V_{sec1} .

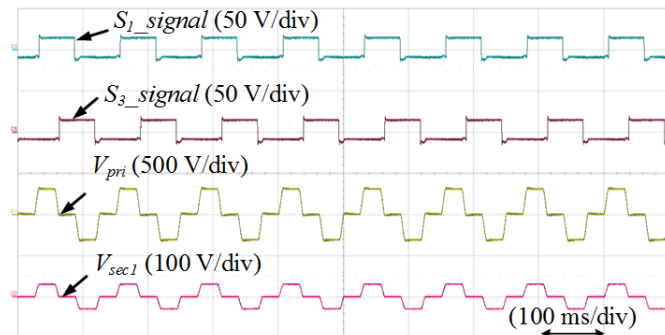


Figure 14. Experimental results about operation principle of the PSFB-CT converter.

Figure 15 shows the experimental results of the PSFB-CT converter using the SMC depending on the K_{SMC} , which was set to (a) 1 and (b) 3, respectively. The V_{out}^* was changed to 15 V from 10 V and the V_{out} was controlled to V_{out}^* . In the case that the SMC is used for the PSFB-CT converter, the dynamic characteristic is improved depending on the K_{SMC} . In Figure 12a,b with the K_{SMC} as 1 and 3, the settling time was about 242 ms and 131 ms, respectively. However, in the steady state, the output voltage and current ripple were increased, which can make system unstable.

In the same scenario as that in Figure 15, Figure 16 shows the experimental results of the PSFB-CT converter using three different controllers: (a) the PI controller, (b) SMC, and (c) proposed hybrid fuzzy SMC. In Figure 16a with the PI controller, the dynamic characteristic of the PSFB-CT converter was undesirable, where the settling time was about 316 ms, which is relatively long. In the steady state, the output voltage ripple was almost zero and the output current ripple was relatively small. In Figure 16b with the SMC, the dynamic characteristic of the PSFB-CT converter was improved where the settling time was roughly 131 ms in comparison to the PI controller. However, in the steady state, the output voltage and current ripple are increased by the chattering phenomenon. In the proposed hybrid fuzzy SMC as shown in Figure 16c, the dynamic characteristic of the PSFB-CT converter was also improved, where the settling time was roughly 161 ms when compared to the PI controller. In addition, in contrast

to the SMC as shown in Figure 16b, the output voltage and current ripple were relatively small. As a result, by properly varying the K_{SMC} depending on the output voltage error in the proposed hybrid fuzzy SMC, the dynamic characteristic is improved and the output voltage and current ripple are decreased in the steady state.

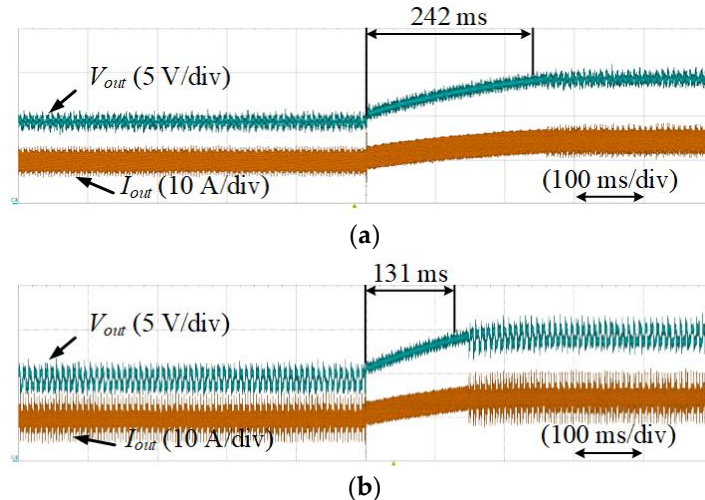


Figure 15. Experimental results of the PSFB-CT converter using the SMC depending on K_{SMC} . (a) $K_{SMC} = 1$; (b) $K_{SMC} = 3$.

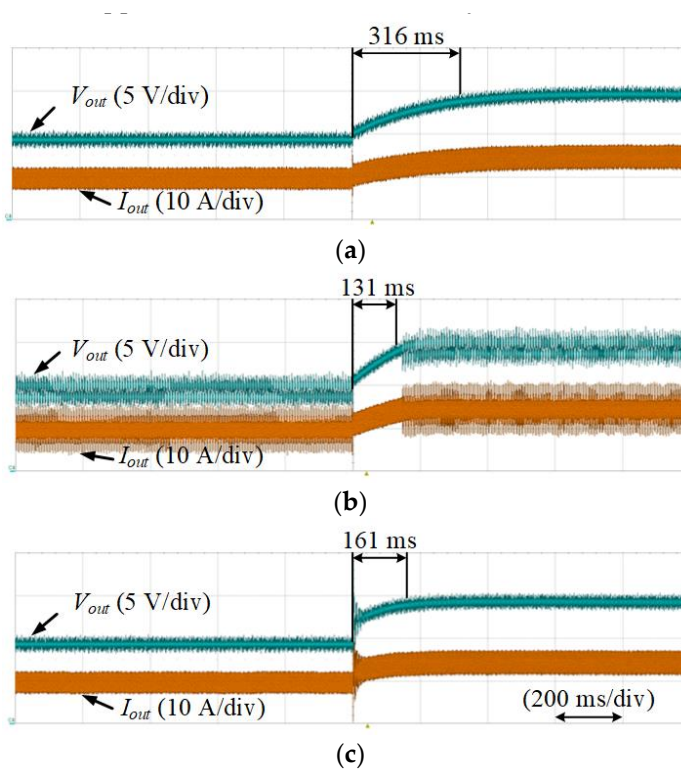


Figure 16. Experimental results of the PSFB-CT converter using three different controllers. (a) the PI controller; (b) SMC; and (c) proposed hybrid fuzzy SMC.

6. Conclusions

This paper proposed a control method for the PSFB-CT converter using the hybrid fuzzy SMC. The dynamic characteristic of the PSFB-CT converter could be improved by using the conventional

SMC compared to the PI controller. However, in the case where the gain of the SMC increased to improve the dynamic characteristic, the output voltage and current ripple caused by the chattering phenomenon were increased in the steady state. In the proposed control method, the gain of the SMC is properly varied by using the fuzzy logic control depending on the output voltage error. Therefore, the dynamic characteristic of the PSFB-CT converter is improved and the output voltage and current ripple are decreased by varying the gain of the SMC. Additionally, through the proposed hybrid fuzzy SMC, a system including the imprecise data and nonlinear function of arbitrary complexity can be handled. The effectiveness of the proposed hybrid fuzzy SMC was verified by the simulation and experimental results.

Author Contributions: K.-B.L. provided guidance and supervision. Y.B. conceived the idea of this paper and performed the simulation. Y.J.L. implemented the main research, performed the experiment, wrote the paper and revised the manuscript as well. All authors have equally contributed to the simulation analysis, experiment and result discussions.

Funding: This work was supported by the Korea Institute of Energy Technology Evaluation and Planning (KETEP) grant funded by the Korea government (MOTIE) (No.20182410105160) and “Human Resources Program in Energy Technology” of the Korea Institute of Energy Technology Evaluation and Planning (KETEP), granted financial resource from the Ministry of Trade, Industry & Energy, Republic of Korea. (No. 20194030202370).

Acknowledgments: Autors thank our Power Electronics Laboratory colleagues of Electrical & Computer Engineering Department, Ajou University, South Korea.

Conflicts of Interest: The authors declare no conflict of interest.

References

1. Kim, S.; Kang, F.-S. Multifunctional onboard battery charger for plug-in electric vehicles. *IEEE Trans. Ind. Electron.* **2015**, *62*, 3460–3472.
2. Kim, D.-H.; Kim, M.-J.; Lee, B.-K. An integrated battery charger with high power density and efficiency for electric vehicles. *IEEE Trans. Power Electron.* **2017**, *32*, 4553–4565. [[CrossRef](#)]
3. Moon, D.; Park, J.; Choi, S. New interleaved current-fed resonant converter with significantly reduced high current side output filter for EV and HEV applications. *IEEE Trans. Power Electron.* **2015**, *30*, 4264–4271. [[CrossRef](#)]
4. Kim, Y.-S.; Jung, D.-W.; Lee, B.-K. Advanced LDC test bed using energy recovery technique for HEVs. *J. Electr. Eng. Technol.* **2013**, *8*, 911–919. [[CrossRef](#)]
5. Lee, S.-R.; Lee, J.-Y.; Jung, W.-S.; Won, I.-K.; Bae, J.-H.; Won, C.-Y. Design and control method of ZVT interleaved bidirectional LDC for mild-hybrid electric vehicle. *J. Electr. Eng. Technol.* **2018**, *13*, 226–239.
6. Kim, Y.-S.; Oh, C.-Y.; Sung, W.-Y.; Lee, B.-K. Topology and control scheme of OBC-LDC integrated power unit for electric vehicles. *IEEE Trans. Power Electron.* **2017**, *32*, 1731–1743. [[CrossRef](#)]
7. Hwu, K.I.; Peng, T.J. A novel buck-boost converter combining KY and buck converters. *IEEE Trans. Power Electron.* **2012**, *27*, 2236–2241. [[CrossRef](#)]
8. Kim, J.-K.; Choi, S.-W.; Kim, C.-E.; Moon, G.-W. A new standby structure using multi-output full-bridge converter integrating flyback converter. *IEEE Trans. Ind. Electron.* **2011**, *58*, 4763–4767. [[CrossRef](#)]
9. Wang, Q.; Cheng, M.; Zhang, B. An improved topology for the current fed parallel resonant half bridge circuits used in fluorescent lamp electronic ballasts. *J. Power Electron.* **2015**, *15*, 567–575. [[CrossRef](#)]
10. Ekkaravarodme, C.; Jirasereamornkul, K. Analysis and implementation of a half bridge class-DE rectifier for front-end ZVS push-pull resonant converters. *J. Power Electron.* **2013**, *13*, 626–635. [[CrossRef](#)]
11. Zhang, T.; Fu, J.; Qian, Q.; Sun, W.; Lu, S. Dead-time for zero-voltage-switching in battery chargers with the phase-shifted full-bridge topology: Comprehensive theoretical analysis and experimental verification. *J. Power Electron.* **2016**, *16*, 425–435. [[CrossRef](#)]
12. Kundu, U.; Yenduri, K.; Sensarma, P. Accurate ZVS analysis for magnetic design and efficiency improvement of full-bridge LLC resonant converter. *IEEE Trans. Power Electron.* **2017**, *32*, 1703–1706. [[CrossRef](#)]
13. Safaee, A.; Jain, P.; Bakhshai, A. A ZVS pulsedwidth modulation full-bridge converter with a low-RMS-current resonant auxiliary circuit. *IEEE Trans. Power Electron.* **2016**, *31*, 4031–4047. [[CrossRef](#)]
14. Wang, H.; Shang, M.; Khaligh, A. A PSFB-based integrated PEV onboard charger with extended ZVS range and zero duty cycle loss. *IEEE Trans. Ind. Appl.* **2017**, *53*, 585–595. [[CrossRef](#)]

15. Bai, H.; Nie, Z.; Mi, C.C. Experimental comparison of traditional phase-shift, dual-phase-shift, and model-based control of isolated bidirectional DC–DC converters. *IEEE Trans. Power Electron.* **2010**, *25*, 1444–1449. [[CrossRef](#)]
16. Shi, K.; Zhang, D.; Zhou, Z.; Zhang, M.; Zhang, D.; Gu, Y. A novel phase-shift dual full-bridge converter with full soft-switching range and wide conversion range. *IEEE Trans. Power Electron.* **2016**, *31*, 7747–7760. [[CrossRef](#)]
17. Xie, L.; Ruan, X.; Ye, Z. Reducing common mode noise in phase-shifted full-bridge converter. *IEEE Trans. Ind. Electron.* **2018**, *65*, 7866–7877. [[CrossRef](#)]
18. Shu, L.; Chen, W.; MA, D.; Ning, G. Analysis of strategy for achieving zero-current switching in full-bridge converters. *IEEE Trans. Ind. Electron.* **2018**, *65*, 5509–5517. [[CrossRef](#)]
19. Liu, J.; Xiao, F.; Ma, W.; Fan, X.; Chen, W. PWM-based sliding mode controller for three-level full-bridge DC–DC converter that eliminates static output voltage error. *J. Power Electron.* **2015**, *15*, 378–388. [[CrossRef](#)]
20. Zheng, K.; Zhang, G.; Zhou, D.; Li, J.; Yin, S. Modeling, dynamic analysis and control design of full-bridge LLC resonant converters with sliding-mode and PI control scheme. *J. Power Electron.* **2018**, *18*, 766–777.
21. Kim, J.-H.; Jou, S.-T.; Choi, D.-K.; Lee, K.-B. Direct power control of three-phase boost rectifiers by using a sliding-mode scheme. *J. Power Electron.* **2013**, *13*, 1000–1007. [[CrossRef](#)]
22. Shahnazi, R.; Shanechi, H.M.; Pariz, N. Position control of induction and DC servomotors: A novel adaptive fuzzy PI sliding mode control. *IEEE Trans. Energy Convers.* **2008**, *23*, 138–147. [[CrossRef](#)]
23. Bandyopadhyay, B.; Gandhi, P.S.; Kurode, S. Sliding mode observer based sliding mode controller for slosh-free motion through PID scheme. *IEEE Trans. Ind. Electron.* **2009**, *56*, 3432–3442. [[CrossRef](#)]
24. Zhang, X.; Sun, L.; Zhao, K.; Sun, L. Nonlinear speed control for PMSM system using sliding-mode control and disturbance compensation techniques. *IEEE Trans. Power Electron.* **2013**, *28*, 1358–1365. [[CrossRef](#)]
25. Chang, E.-C.; Cheng, H.-L.; Liao, K.-Y. Design of adaptive fuzzy sliding-mode PI control for full-bridge inverters. In Proceedings of the 2014 International Conference on Fuzzy Theory and Its Applications, Kaohsiung, Taiwan, 26–28 November 2014; pp. 144–147.
26. Kim, T.-H.; Lee, S.-J.; Choi, W. Design and control of the phase shift full bridge converter for the on-board battery charger of electric forklifts. *J. Power Electron.* **2012**, *12*, 113–119. [[CrossRef](#)]
27. Cetin, S. High efficiency design considerations for the self-driven synchronous rectified phase-shifted full-bridge converters of server power systems. *J. Power Electron.* **2015**, *15*, 634–643. [[CrossRef](#)]
28. Wu, X.; Xie, X.; Zhao, C.; Qian, Z.; Zhao, R. Low voltage and current stress ZVZCS full bridge DC–DC converter using center tapped rectifier reset. *IEEE Trans. Ind. Electron.* **2008**, *55*, 1470–1477. [[CrossRef](#)]
29. Zhang, J.; Shi, P.; Xia, Y. Robust adaptive sliding-mode control for fuzzy systems with mismatched uncertainties. *IEEE Trans. Fuzzy Syst.* **2010**, *18*, 700–711. [[CrossRef](#)]
30. Hung, J.Y.; Gao, W.; Hung, J.C. Variable structure control: A survey. *IEEE Ind. Electron.* **1993**, *40*, 2–22. [[CrossRef](#)]
31. Torok, L.; Munk-Nielsen, S. Digital fuzzy logic and PI control of phase-shifted full-bridge current-doubler converter. In Proceedings of the IEEE 2011 International Telecommunications Energy Conference, Amsterdam, Netherlands, 9–13 October 2011; pp. 978–984.
32. Wang, W.; Shi, Y.; Yang, D. A new modeling method for the switching power converter. In Proceedings of the IEEE 2008 Workshop on Power Electronics and Intelligent Transportation System, Guangzhou, China, 2–3 August 2008; pp. 404–407.
33. Valdivia, V.; Barrado, A.; Lazaro, A.; Zumel, P.; Raga, C.; Fernandez, C. Simple modeling and identification procedures for “Black-Box” behavioral modeling of power converters based on transient response analysis. *IEEE Trans. Power Electron.* **2009**, *24*, 2776–2790. [[CrossRef](#)]
34. Rubaai, A.; Ofoli, A.R.; Burge, L.; Garuba, M. Hardware implementation of an adaptive network-based fuzzy controller for DC–DC converters. *IEEE Trans. Ind. Appl.* **2005**, *41*, 1557–1565. [[CrossRef](#)]
35. Aghili-Ashtiani, A.; Menhaj, M.B. Introducing the fuzzy relational hybrid model as a building block for intelligent modeling of hybrid dynamical systems. *IEEE Trans. Fuzzy Syst.* **2015**, *23*, 1971–1983. [[CrossRef](#)]
36. Ro, H.-S.; Lee, K.-G.; Lee, J.-S.; Jeong, H.-G.; Lee, K.-B. Torque ripple minimization scheme using torque sharing function based fuzzy logic control for a switched reluctance motor. *J. Electr. Eng. Technol.* **2015**, *10*, 118–127. [[CrossRef](#)]
37. Hu, H.; Woo, P.-Y. Fuzzy supervisory sliding-mode and neural-network control for robotic manipulators. *IEEE Trans. Ind. Electron.* **2006**, *53*, 929–940. [[CrossRef](#)]

38. Mi, Y.; Zhang, H.; Fu, Y.; Wang, C.; Loh, P.C.; Wang, P. Intelligent power sharing of DC isolated microgrid based on fuzzy sliding mode droop control. *IEEE Trans. Smart Grid* **2019**, *10*, 2396–2406. [[CrossRef](#)]
39. Runkler, T.A. Selection of appropriate defuzzification methods using application specific properties. *IEEE Trans. Fuzzy Syst.* **1997**, *50*, 72–79. [[CrossRef](#)]
40. Chang, Y.-C.; Chen, S.-M.; Liau, C.-J. Fuzzy interpolative reasoning for sparse fuzzy-rule-based systems based on the areas of fuzzy sets. *IEEE Trans. Fuzzy Syst.* **2008**, *16*, 1285–1301. [[CrossRef](#)]
41. Zhao, J.; Bose, B.K. Evaluation of membership functions for fuzzy logic controlled induction motor drive. In Proceedings of the IEEE 2018 Annual Conference of the Industrial Electronics Society, Sevilla, Spain, 5–8 November 2018; pp. 229–243.



© 2019 by the authors. Licensee MDPI, Basel, Switzerland. This article is an open access article distributed under the terms and conditions of the Creative Commons Attribution (CC BY) license (<http://creativecommons.org/licenses/by/4.0/>).